

**A Further Measurement of the  $\beta$ -Delayed  $\alpha$ -Particle Emission of**  
 $^{16}\text{N}^*$

R.H. France III<sup>†</sup>

*Department of Chemistry & Physics, Campus Box 82,  
Georgia College & State University, Milledgeville, Georgia 31061*

E.L. Wilds

*Division of Radiation Safety, Connecticut-DEP,  
79 Elm Street, Hartford, CT 06106*

J.E. McDonald

*Department of Physics, University of Hartford,  
200 Bloomfield Avenue, West Hartford, CT 06117-1599*

M. Gai

*Laboratory for Nuclear Sciences at Avery Point,  
University of Connecticut,  
1084 Shennecossett Road,  
Groton, CT 06340-6097.*

*and*

*Department of Physics,  
WNSL-102, P.O. Box 208124,  
Yale University, 272 Whitney Avenue,  
New Haven, CT 06520-8124.*

## Abstract

We measured the  $\beta$ -delayed  $\alpha$ -particle emission spectrum of  $^{16}\text{N}$  with a sensitivity for  $\beta$ -decay branching ratios of the order of  $10^{-10}$ . The  $^{16}\text{N}$  nuclei were produced using the  $d(^{15}\text{N}, ^{16}\text{N})p$  reaction with 70 MeV  $^{15}\text{N}$  beams and a deuterium gas target 7.5 cm long at a pressure of 1250 torr. The  $^{16}\text{N}$  nuclei were collected (over 10 s) using a thin aluminum foil with an areal density of  $180 \mu\text{g}/\text{cm}^2$  tilted at  $7^\circ$  with respect to the beam. The activity was transferred to the counting area by means of a stepping motor in less than 3 s with the counting carried out over 8 s. The  $\beta$ -delayed  $\alpha$ -particles were measured using a time of flight method to achieve a sufficiently low background. Standard calibration sources ( $^{148}\text{Gd}$ ,  $^{241}\text{Am}$ ,  $^{208,209}\text{Po}$ , and  $^{227}\text{Ac}$ ) as well as alpha-particles and  $^7\text{Li}$  from the  $^{10}\text{B}(n, \alpha)^7\text{Li}$  reaction were used for an accurate energy calibration. The energy resolution of the catcher foil (180-220 keV) was calculated and the time of flight resolution (3-10 nsec) was measured using the  $\beta$ -delayed  $\alpha$ -particle emission from  $^8\text{Li}$  that was produced using the  $d(^7\text{Li}, ^8\text{Li})p$  reaction with the same setup. The line shape was corrected to account for the variation in the energy and time resolution and a high statistics spectrum of the  $\beta$ -delayed  $\alpha$ -particle emission of  $^{16}\text{N}$  is reported. However, our data (as well as earlier Mainz data and unpublished Seattle data) do not agree with an earlier measurement of the  $\beta$ -delayed  $\alpha$ -particle emission of  $^{16}\text{N}$  taken at TRIUMF after averaging over the energy resolution of our collection system. This disagreement, amongst other issues, prohibits accurate inclusion of the f-wave component in the R-matrix analysis.

PACS numbers: 26.20.+f 97.10.Cv 98.80.Ft 23.60.+e 23.40.-s

---

\*Supported by USDOE grants No. DE-FG02-91ER40609 and DE-FG02-94ER40870

†Also at: A.W. Wright Nuclear Structure Laboratory, P.O. Box 208124, Yale University, 272 Whitney Avenue, New Haven, CT 06520-8124

## I. INTRODUCTION

The  $^{12}\text{C}(\alpha, \gamma)^{16}\text{O}$  reaction is of critical importance for understanding stellar evolution [1]. It competes with the  $^8\text{Be}(\alpha, \gamma)^{12}\text{C}$  reaction (that forms carbon) to yield oxygen during stellar helium burning, together determining the carbon/oxygen (C/O) ratio at the end of helium burning. The C/O ratio is of major importance for understanding type II [2] and apparently also the light curve of type Ia [3] supernovae. Since the  $^8\text{Be}(\alpha, \gamma)^{12}\text{C}$  reaction is comparatively well known ( $\pm 12\%$ ), the  $^{12}\text{C}(\alpha, \gamma)^{16}\text{O}$  reaction provides the principle uncertainty in the C/O ratio at the end of helium burning.

The  $\beta$ -delayed  $\alpha$ -particle emission of  $^{16}\text{N}$  (*i.e.*  $\alpha$ -particles emitted from the continuum of  $^{16}\text{O}$  populated by the  $\beta$ -decay of  $^{16}\text{N}$ ) has been predicted to provide a constraint on the cross section of this reaction [4, 5, 6, 7], but it requires a measurement of a  $\beta$ -decay of  $^{16}\text{N}$  with a sensitivity for a Branching Ratio (BR) of the order of  $10^{-9}$ . In particular, the low energy portion of the alpha-particle spectrum has been predicted to be sensitive to the reduced  $\alpha$ -particle width of the bound  $1^-$  state in  $^{16}\text{O}$ ; however, it cannot directly determine the mixing phase in the  $^{12}\text{C}(\alpha, \gamma)^{16}\text{O}$  reaction of the two interfering states at  $7.12\text{ MeV}$  and  $9.58\text{ MeV}$  in  $^{16}\text{O}$ .

In the early 1970s F.C. Barker [4, 5] proposed the use of the  $\beta$ -delayed  $\alpha$ -particle emission spectrum of  $^{16}\text{N}$  to constrain  $S_{E1}$ , the p-wave component of the astrophysical cross section factor. At the time of these calculations [4, 5], a single  $\beta$ -delayed  $\alpha$ -particle emission spectrum with very high statistics ( $> 36$  million counts) existed. These data were measured at Mainz [8, 9, 10] in a successful measurement of the parity violating  $1.281\text{ MeV}$   $\alpha$ -particle decay. However, these data were only listed in numerical form in private communications [11]. Unfortunately, this spectrum excluded the energy region of the interference peak predicted at  $1.1\text{ MeV}$ .

In the early 1990s three additional measurements of this spectrum were made: at TRIUMF [12], at Yale [13, 14], and at the University of Washington at Seattle (unpublished) [15]. The experiment reported here [16, 17] is a continuation and improvement of the original Yale-UConn experiment [13, 14]. We refer the reader to the appendix of Ref. [17] where all available data from each of these experiments, including the unpublished Seattle experiment [15] and the old Mainz experiment [8, 9, 10], are listed in tabular form.

Recently a renewed interest in the spectrum of the  $\beta$ -delayed  $\alpha$ -particle emission of  $^{16}\text{N}$

## Experimental Setup

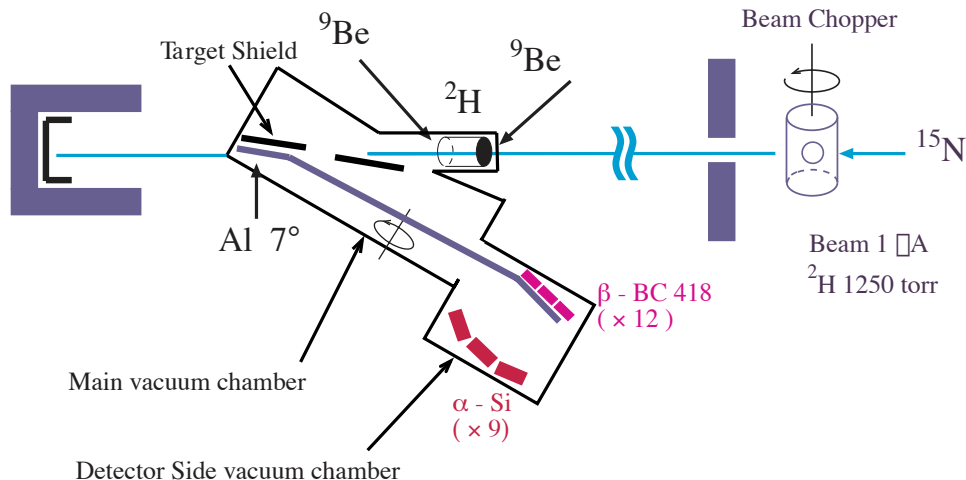


FIG. 1: Diagram of the experimental setup showing the rotating arm and the two stations (collection and counting). The beam chopper is far upstream and is well shielded from the experimental hall where the data were collected. Figure is not drawn to scale.

has been generated by a new experiment carried out at the Argonne National Lab [18]. The primary purpose of this paper is to publish a detailed account of the data from our improved experiment that were already shown in the literature [16]. In addition we include in the appendix of this paper the same numerical listing as included (by permission) in Ref. [17] of the Seattle data [15] as well as the Mainz data [8, 9, 10]. The Seattle and Mainz data have been repeatedly discussed by a number of authors that quoted Reference [17] as the source for these data, and we consider it advantageous to list it here in numerical form. We compare these data sets and demonstrate that our data agrees with the Mainz and Seattle data but not with the TRIUMF data. We also note that the preliminary reported data of the Argonne group [18] agree with our data. We discuss the relevance of this disagreement for the global R-matrix fit of the data.

## II. EXPERIMENTAL PROCEDURES

The experiments were performed using  $150 - 250 \text{ pA } 70 \text{ MeV } ^{15}\text{N}$  beams from the Yale ESTU tandem van de Graff accelerator and a deuterium gas target to produce  $^{16}\text{N}$  using the  $d(^{15}\text{N}, ^{16}\text{N})p$  reaction. The produced  $^{16}\text{N}$  nuclei emerged from the gas target and were

stopped in aluminum catcher foils, as shown in Fig. 1. These foils were then rotated into a counting area to measure the decays of  $^{16}\text{N}$ . The use of reversed kinematics allowed for the  $^{16}\text{N}$  to be kinematically focussed into a forward cone of about  $7^\circ$ . The  $^{16}\text{N}$  nuclei were implanted into thin aluminum catcher foils located at the ends of an approximately 1 m long arm which rotated about its center. After each production cycle, the arm rotated  $180^\circ$ , placing the implanted catcher foil between two detector arrays which measured the beta and alpha-particles in coincidence.

We used a deuterium gas target, composed of a copper cylinder 7.5 cm long and 1.9 cm in diameter with 0.3 cm thick walls cooled with an alcohol cooling system to  $-40^\circ\text{C}$ . Thin beryllium pressure foils (25  $\mu\text{m}$ ) were attached with Araldite AW 106/HV 953 epoxy from CIBA-GEIGI (good for very low temperatures) to the ends of the cylinder. To reduce plural scattering, beryllium was chosen for the pressure windows as it has a low  $Z$  ( $Z = 4$ ). The target was filled with approximately 1250 torr of deuterium gas and was placed close to the catcher foils with its exit window only 7.5 cm from the edge of the catcher foil.

The  $^{16}\text{N}$  emerged from the target with a broad distribution of energies (of order 7 MeV) of which the catcher foils collected the lowest 1 MeV portion. To allow the capture of these ions while retaining useful  $\alpha$ -particle energy resolution, the catcher foils were made of thin (180  $\mu\text{g}/\text{cm}^2$ ) aluminum tilted at  $7^\circ$  with respect to the beam, see Fig. 1, to increase their effective catching thickness by a factor of 8.

The foils were attached to aluminum frames with epoxy and had open areas of 5 cm  $\times$  20 cm. Inside the chamber, see Fig. 1, a tantalum shield was positioned less than 1 mm from the catcher foil to prevent  $^{16}\text{N}$  from hitting the catcher frames. Very precise alignment of the shields and catcher foils was necessary to ensure that the  $^{16}\text{N}$  was stopped in the catcher foils and not elsewhere, where it would produce a low energy tail in the alpha-particle spectrum. The alignment was tested using empty catcher foil frames. The  $^{15}\text{N}$  beam was confined to travel through the system using two sets of beam defining slits: one slit located several meters upstream and the second one about a meter upstream. The beam position was also constrained by two additional tantalum collimators, the target itself, and the shield, discussed above.

During the collection period the neutron background was very large hence the data acquisition system was turned off during irradiation. The experiments were run in 21 second cycles, to maximize detection efficiency given the 10 second lifetime of  $^{16}\text{N}$ . The first 10

seconds of each cycle was the production period during which the  $^{16}\text{N}$  was produced in the target and collected in the catcher foils. At the end of this time, a tantalum beam chopper blocked the beam far upstream followed by the arm carrying the catcher foil rotating  $180^\circ$  in slightly less than 3 s. Three seconds after the rotation began, the data acquisition system was activated for 8 s. In order to protect the catcher foil frames from the beam, the position of the beam chopper was read back into the control room, and the arm rotation did not begin until the beam chopper was fully in place. Since catcher foils were located at both ends of the arm, it was not necessary to rotate the arm at the end of the cycle and a second (10 s) collection period commenced.

The principle detectors in this experiment were nine Silicon Surface Barrier (SSB) detectors located in a square array and used to detect  $\alpha$ -particles. Each detector had an active area of  $450\text{ mm}^2$  and a  $50\text{ }\mu\text{m}$  thick active region to minimize deposition of energy from  $\beta$ -particles. Canberra 2003B preamps, which had been modified to match the high capacitance of the detectors, were used. The measured energy resolution of the detectors was about  $55\text{ keV}$ , and the array was located  $83\text{ mm}$  from the catcher foil.

The secondary detector array (the  $\beta$ -array) was composed of twelve plastic scintillation detectors made of BC418 fast plastic scintillator and Hamamatsu H3165 and H3171 photomultipliers and was used to detect  $\beta$ -particles. The central six detectors were  $2.5 \times 2.5 \times 0.6\text{ cm}$ , while the outer six detectors were  $5.0 \times 5.0 \times 0.6\text{ cm}$ . The detectors were optically isolated from one another using aluminum foil and were covered by a  $0.02\text{ mm}$  aluminized mylar film to prevent the detection of  $\alpha$ -particles or  $^{12}\text{C}$  recoils. The  $\beta$ -array subtended approximately 30% of  $4\pi$ , as shown in Fig. 1.

The data were collected event by event and written to Exabyte tapes by a Concurrent 3230 computer running the Oak Ridge data acquisition system [17]. Each event was started by one of the  $\alpha$ -detectors firing. For each  $\beta$ -detector which fired, a delayed relative timing signal was recorded using a Lecroy 2228A time to digital converter. Thus for each event one  $\alpha$ -particle energy and 12  $\alpha$ - $\beta$  relative time measurements were recorded.

The energy calibration of the  $\alpha$ -detectors was performed using  $\alpha$ -particles from five different standard calibration sources:  $^{148}\text{Gd}$ ,  $^{241}\text{Am}$ ,  $^{208}\text{Po}$ ,  $^{209}\text{Po}$ ,  $^{227}\text{Ac}$  and  $\alpha$ -particles as well as  $^7\text{Li}$  emitted in the  $^{10}\text{B}(n, \alpha)^7\text{Li}$  reaction, yielding eleven  $\alpha$ -particle energies from 1.471 MeV to 7.386 MeV. Energy loss in these calibration sources and the  $^{10}\text{B}(n, \alpha)^7\text{Li}$  source were negligible and did not affect the energy calibration. A typical  $^{10}\text{B}(n, \alpha)^7\text{Li}$  calibration

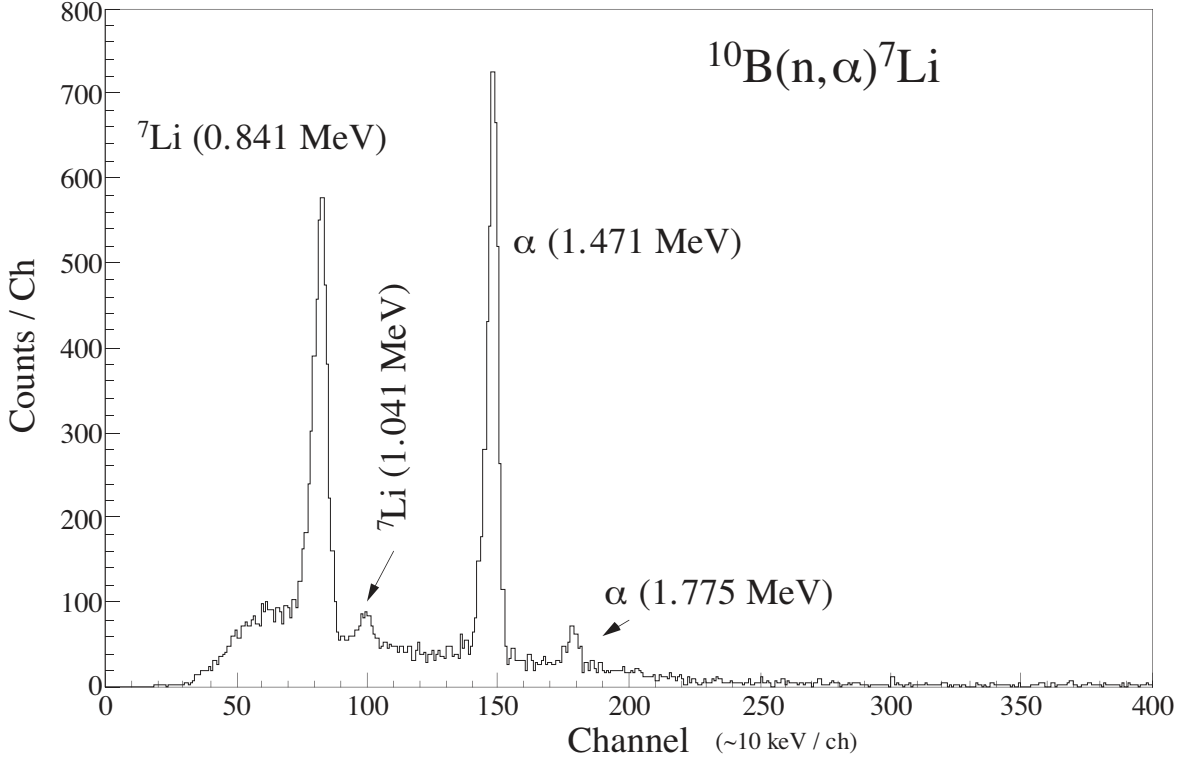


FIG. 2: Typical  $^{10}\text{B}(n, \alpha)^7\text{Li}$  calibration spectrum used in this study.

spectrum is shown in Fig. 2. In addition the detectors were implanted with small amounts of Polonium and Actinium leading to a continuous online energy calibration throughout the experiment. These online calibration lines did not perturb the time of flight coincidence spectra.

### III. DATA ANALYSIS

The detector timing was calibrated using 22 MeV  $^7\text{Li}$  beams and the  $^2\text{H}(^7\text{Li}, ^8\text{Li})^1\text{H}$  reaction. The  $^8\text{Li}$  undergoes  $\beta$ -delayed  $\alpha$ -particle emission with a lifetime just under 1 s. The measured  $^8\text{Li}$  spectra were plotted in 108 (one for each  $\alpha$ - $\beta$  detector pair) two-dimensional histograms with time along the  $x$ -axis and detected  $\alpha$ -particle energy along the  $y$ -axis, as shown in Fig. 3. Each  $^8\text{Li}$  histogram was initially cut into sixteen 100 keV wide slices which were projected onto the time axis, similar to the (50 keV) slices shown in Fig. 4; the resulting 1728 spectra were each fit using the Oak Ridge data analysis program SAMGR with skewed gaussians to determine the time of flight (TOF) peak positions and shapes, see Fig. 4. For each detector pair, these TOF centroids were fit as a function of energy;

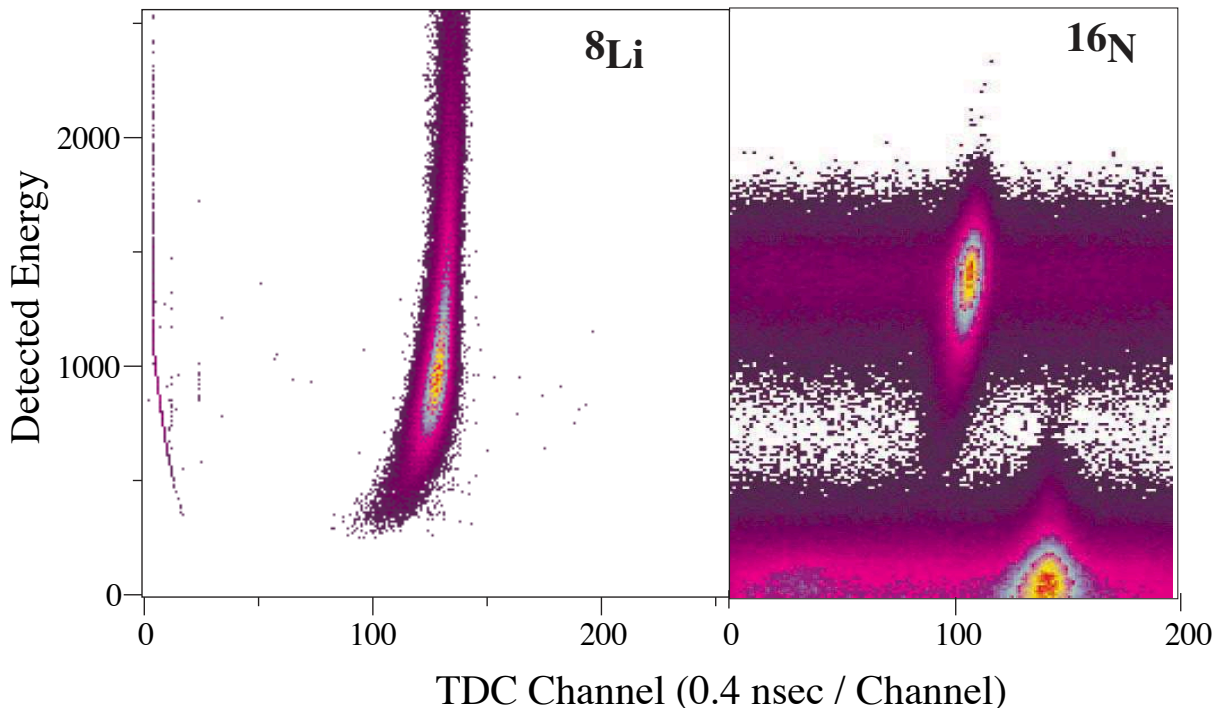


FIG. 3: Typical two dimensional energy *vs.* time of flight spectra for  ${}^8\text{Li}$  and  ${}^{16}\text{N}$  data.

$Centroid = \sqrt{m_\alpha/2 \times Energy} * d + B$  where  $d$  is the distance from the  $\alpha$ -particle source to the detector, as shown in Fig. 5. The fitted values of  $d$  were consistent with the distances measured directly (about 8.3 cm). The obtained time of flight parameters were used for matching the  ${}^{16}\text{N}$  spectra. The time of flight resolution was determined from these  ${}^8\text{Li}$  spectra and the energy resolution was determined by using Ziegler's formulae [19] with the known effective thickness measured *in situ* using a  ${}^{148}\text{Gd}$  source. The time and energy resolutions are shown in Fig. 5.

A  $\beta$ -delayed  $\alpha$ -particle emission spectrum of  ${}^{16}\text{N}$  was obtained with approximately 1.3 million  $\alpha$ -particles in singles using the following procedure. After matching the spectra using the results of the  ${}^8\text{Li}$  calibration as discussed above, the  ${}^{16}\text{N}$  spectra were combined into one two dimensional histogram, as shown in Fig 3. This summed two dimensional spectrum was then cut into 50 keV wide slices which were individually analysed using the Oak Ridge software, see Fig. 4, and corrected for the measured  $\beta$ -particle efficiency of the  $\beta$ -array. One of the  $\beta$ -detectors failed during the experiment and was not used in the analysis. For purely geometric reasons approximately one third of the remaining detector pairings were not used



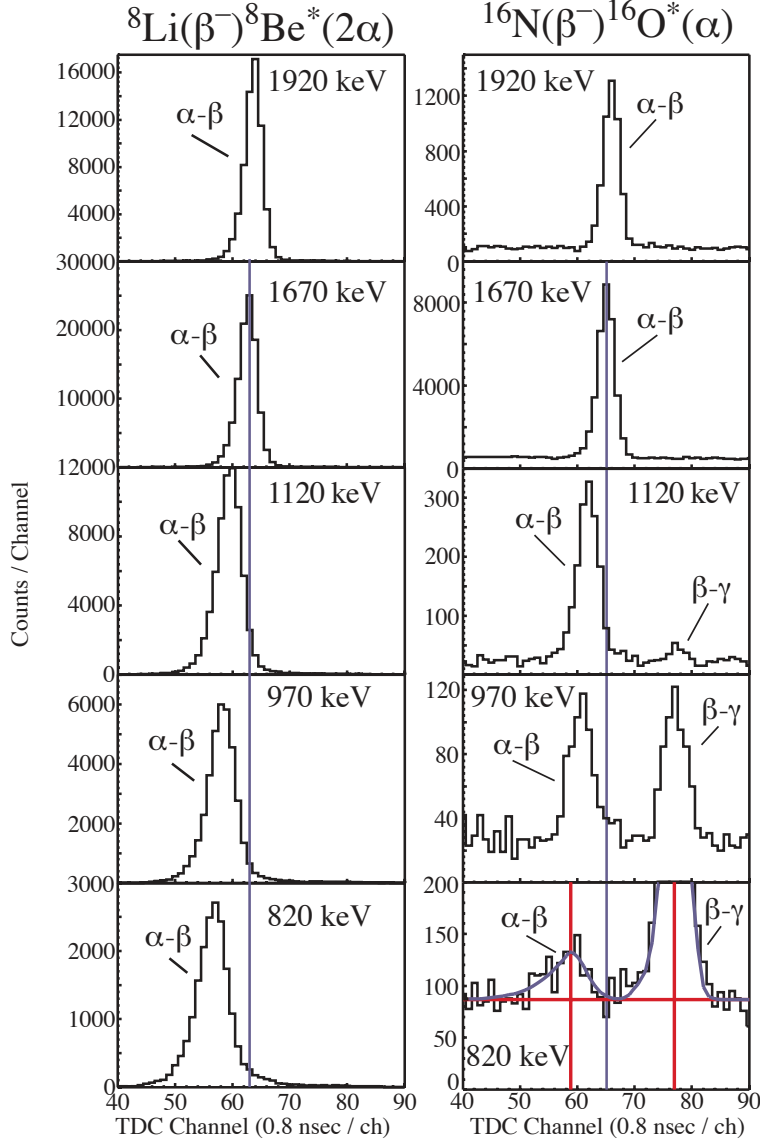


FIG. 4: Typical  $50\text{ keV}$  wide slices from the 2 dimensional  ${}^8\text{Li}$  and  ${}^{16}\text{N}$  energy vs time plots, see Fig. 3, projected upon the time axis. The slices are labeled by the high energy end of the slice from which an effective center of mass energy is determined using the known energy loss. The  $\alpha$ - $\beta$  coincidence peak is well separated from the  $\beta$ - $\gamma$  peak at low energies, and due to the kinematics, is also distinguishable from signals caused by partial charge collection in the  $\alpha$ -detector. The  $1670\text{ keV}$  slice is at the central peak for  ${}^{16}\text{N}$  and the line drawn through it (which represents the expected time of flight location of a low energy tail) is clearly separated from the  $\alpha$ - $\beta$  coincidence peak at lower energies. The  ${}^8\text{Li}$  slices are located at slightly lower channels due to the different leading edge threshold of the higher energy  $\beta$ -particles in the Lithium decay.

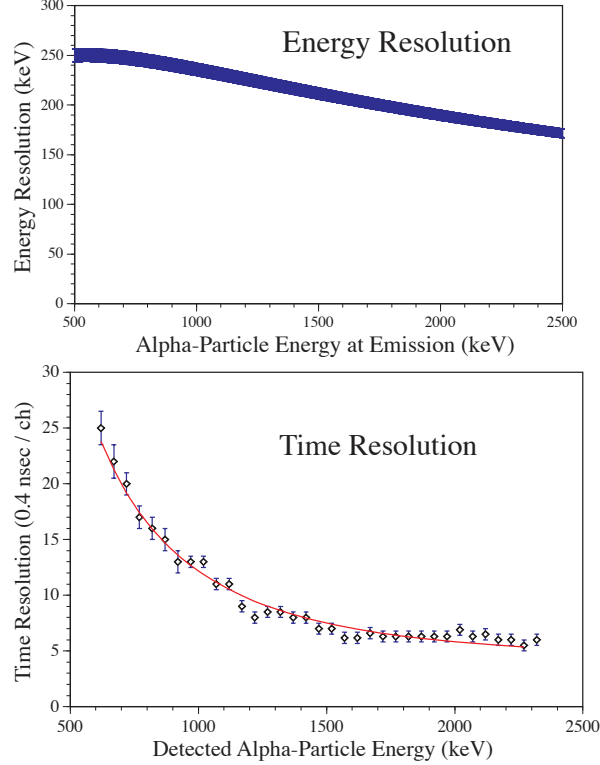


FIG. 5: The energy and time resolution (FWHM) as a function of energy. The energy resolution is determined by the thickness of the aluminum catcher foil in which the  $^{16}\text{N}$  is embedded. The time resolution is based on measurements from the decay of  $^8\text{Li}$ .

in our analysis, as their timing resolutions were insufficient to separate out the background (discussed below).

The effective energy of the emerging  $\alpha$ -particles for each data point was calculated using the expected variation of the yield over the energy width of the catcher foil for each slice. The effective center of mass energy was calculated and is listed as  $E_{cm}$  in Table 1. Note that due to fast variation in the yield, the effective  $\alpha$ -particle energy is not the one due to  $\alpha$ -particles emitted from the center of the catcher foil.

The measured spectral line shape was corrected for distortions caused by the variability of our time and energy resolutions, see Fig. 5. For a spectrum constant in energy, the yield measured at each point in that spectrum is directly proportional to the energy integration interval. This conclusion holds for a spectrum in any physical variable. In the case of this experiment, the data are integrated over both time and energy with the integration intervals being the time and energy resolutions. The fact that these vary considerably over

the energy range of the detected  $\alpha$ -particles causes a significant distortion in the line shape. The data were normalized by dividing by the effective integration intervals, *i.e.* the time and energy resolutions as shown in Fig. 5, to correct this distortion. The energy resolution of the experiment (the thickness of the aluminum catcher foils) is considerably larger than the intrinsic resolution of the SSB detectors. These resolutions are based on the measured time resolutions from the  $^8\text{Li}$  data and the measured thickness of the catcher foils [17] determined by using Ziegler's formulae [19] upon the known effective thickness measured *in situ* using a  $^{148}\text{Gd}$  source. The final spectrum, with these resolutions divided out, is shown in Fig. 6 and listed in tabular form in Table 1.

There are two principle sources of background in this experiment. The first is  $\beta$ - $\gamma$  coincidences; these occur when a  $\beta$ -particle is detected in an  $\alpha$ -detector in coincidence with a  $\gamma$ -ray detected in a  $\beta$ -detector. Most of these  $\beta$ - $\gamma$  coincidences arise from activated  $^{28}\text{Al}$  created by neutron capture on the aluminum capture foils. The second source of background is due to partial charge collection in the SSB. In both cases the background coincidence is well separated from the data due to the fast timing requirements, as shown in Fig 4.

Table 1: The currently measured Yale(96) data.

$E_{cm}$	cts./ch	$E_{cm}$	cts./ch	$E_{cm}$	cts./ch	$E_{cm}$	cts./ch
975	46.1(175)	1563	517.0(313)	2149	19856.7(14335)	2739	5241.7(4095)
1040	67.5(104)	1628	799.5(461)	2215	26832.3(19323)	2804	3082.4(2593)
1105	72.5(114)	1693	1227.0(683)	2280	33244.0(23917)	2869	1700.9(1584)
1171	63.6(95)	1758	1961.1(1500)	2345	36684.7(26388)	2936	958.3(1238)
1236	85.1(95)	1823	2907.9(2183)	2412	35711.0(25700)	3001	479.1(1684)
1301	75.3(84)	1889	4382.8(3244)	2477	29550.8(21319)	3067	238.0(939)
1367	135.2(109)	1853	6725.9(4928)	2542	21181.2(15364)	3132	123.5(906)
1432	207.1(147)	2019	9778.2(7116)	2608	13623.0(9989)		
1497	315.3(206)	2084	14568.2(10545)	2673	8626.0(6462)		

#### IV. DISCUSSION

In addition to our experiment there were three high-statistics data sets for the  $\beta$ -delayed  $\alpha$ -particle emission of  $^{16}\text{N}$ . The first (containing approximately 32 million events) was taken in Mainz, Germany by K. Neubeck *et al.* [10], in a successful measurement of the 1.2825 MeV

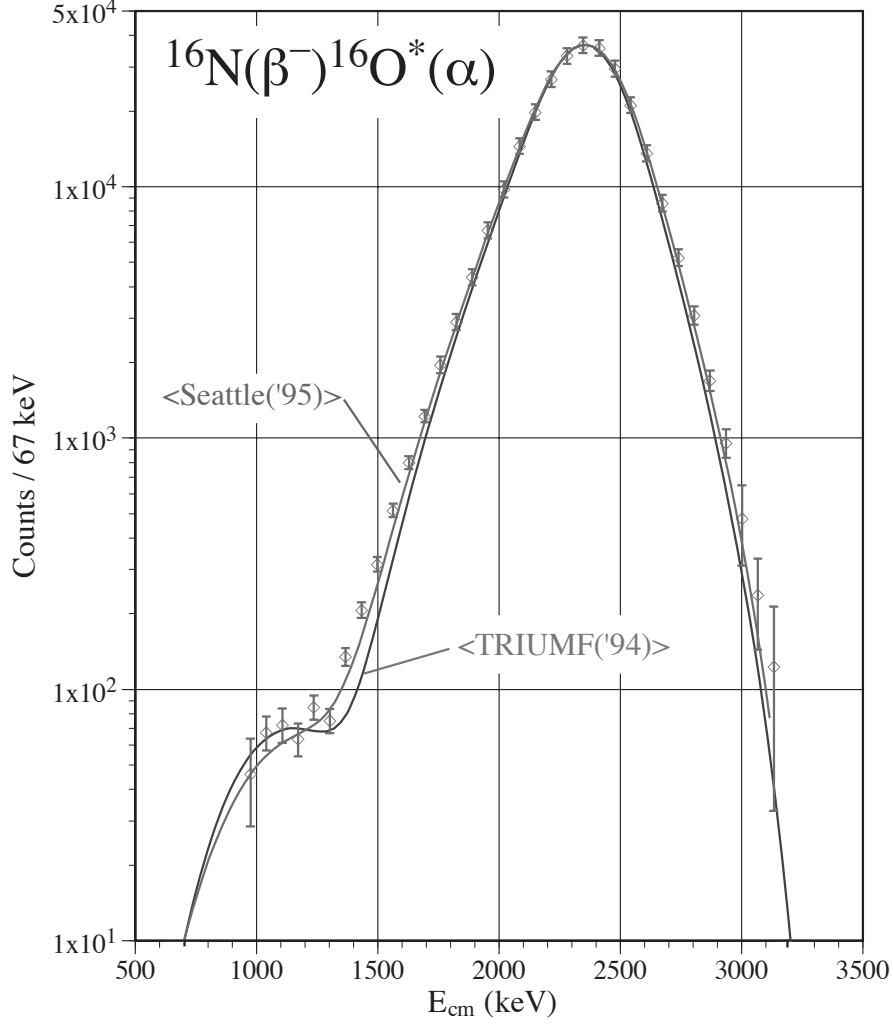


FIG. 6: The  $\beta$ -delayed  $\alpha$ -particle emission spectrum of  $^{16}\text{N}$  obtained in this work. The TRIUMF and Seattle R-Matrix fitted curves [12, 15] averaged over the energy resolution of our experiment (shown in Fig. 5) are compared to our data.

$\alpha$ -particles from the parity violating  $\alpha$ -particle decay of the 8.8719 MeV  $2^-$  state in  $^{16}\text{O}$ . The second (containing approximately 1.25 million events) was taken in the TRIUMF lab in Canada [12]. The third (containing approximately 0.1 million events) was taken at the University of Washington in Seattle, Washington by Z. Zhao *et al.* [15].

Due to the thickness of our catcher foils, the inherent energy resolution of our experiment is significantly poorer than that of the previous experiments. Thus, in order to do a proper

comparison, the previous data sets must be averaged over our variable energy resolution. To do this, the published R-Matrix fitted curves from the Seattle and TRIUMF data sets were used to minimize end-effects in the averaging process. The use of the R-matrix fit curve is appropriate as the fitted curves reproduce the data quite well [12, 15] and it allows us to extend beyond the region of measured data for a meaningful averaging.

In Fig 6 we show a comparison of our data with the averaged fitted curves of Seattle and TRIUMF. Our data agree fairly well with the Seattle averaged fit curve with a  $\chi^2$  per data point of 1.4, while disagreeing with the TRIUMF averaged fit curve with a  $\chi^2$  per data point of 7.2. In Fig. 7 we show a comparison of the Mainz data with the Seattle and TRIUMF fit curves. These three data sets were measured with comparable energy resolution and in this comparison there is no need to employ energy averaging. The Mainz data also agrees with the Seattle fit curve with a  $\chi^2$  per data point of 2.5, while badly disagreeing with the TRIUMF fit curve with a  $\chi^2$  per data point of 123.

The disagreement with the TRIUMF data is manifestly due to a difference in the width of the primary peak, and not in the height of the secondary low energy peak. The agreement on the height of the low energy peak in and of itself demonstrates the viability of the time of flight method used in this experiment and negates a claim of a low energy tail in our data. The disagreement could quite possibly be due to over subtraction of  $^{18}\text{N}$  contamination in the TRIUMF data.

In the case of  $\beta$ -delayed  $\alpha$ -particle emission of  $^{16}\text{N}$  the R-matrix fit includes an additional partial wave, the f-wave, that affects the  $^{16}\text{N}$  results, while not playing any role in the astrophysical  $^{12}\text{C}(\alpha, \gamma)^{16}\text{O}$  reaction. The f-wave component is determined primarily through the depth of the interference minimum around 1.4 MeV, which is also dependent upon the width of the primary peak. The disagreement in the region of the interference minimum around 1.4 MeV is sufficient to change the f-wave component and leads to imprecise determination of the p-wave contribution to the  $^{16}\text{N}$  spectrum.

## V. CONCLUSION

We report on our improved measurement of the  $\beta$ -delayed  $\alpha$ -particle emission of  $^{16}\text{N}$  with results that are in agreement with the old Mainz data and the new unpublished Seattle data but in disagreement with the TRIUMF data. The disagreements are entirely caused

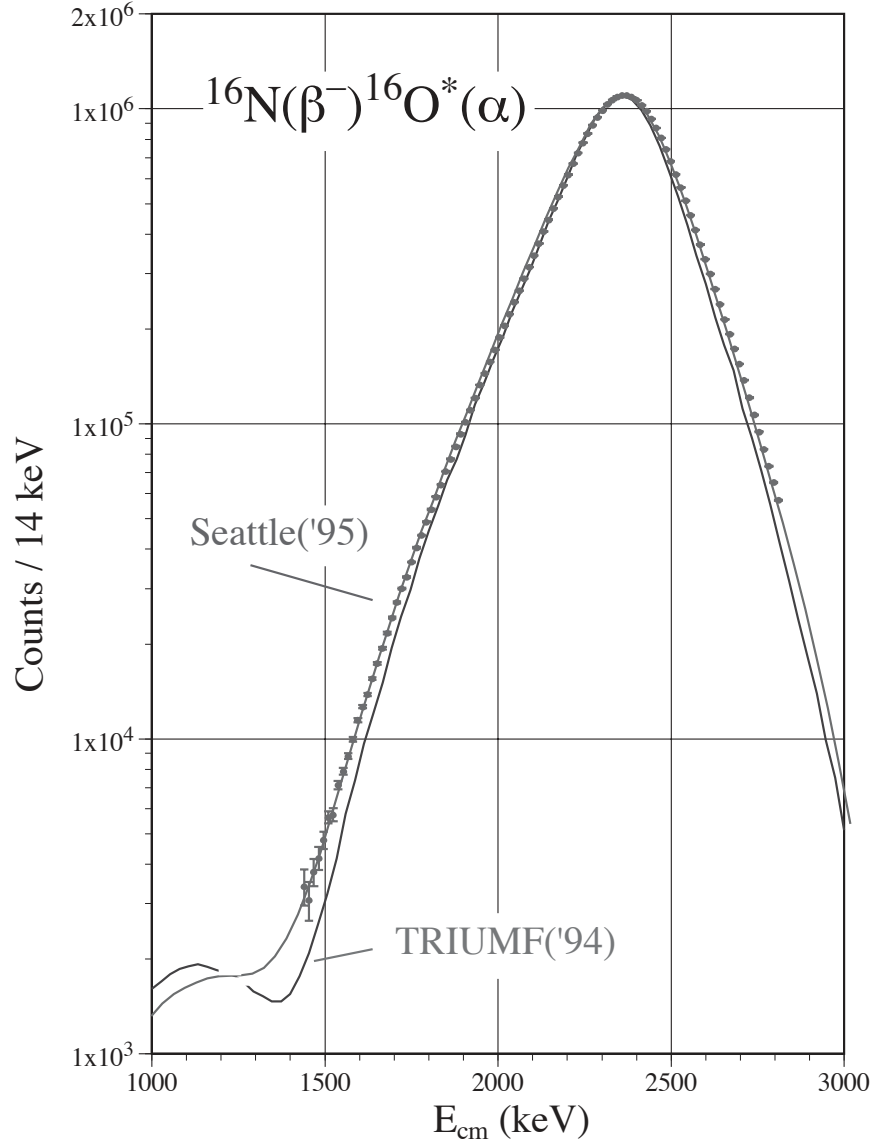


FIG. 7: TRIUMF and Seattle R-Matrix fitted curves [12, 15] compared with the Mainz data [8, 9, 10, 11].

by differences in the width of primary peak and the depth of the interference minimum. Without precise knowledge of this minimum, the f-wave component cannot be determined with high accuracy and the corresponding p-wave spectrum cannot be extracted with high precision.

---

[1] W.A. Fowler; Rev. Mod. Phys., **58**(1984)149.

- [2] T.A. Weaver and S.E. Woosley, Phys. Rep. **227**(1993)65.
- [3] P. Höflich and J. Stein. ApJ., **568**(2002)779.
- [4] F.C. Barker. Aust. J. Phys., **22**(1969)293.
- [5] F.C. Barker. Aust. J. Phys., **24**(1971)777.
- [6] X. Ji, B.W. Fillippone, J. Humblet, and S.E. Koonin. Phys. Rev. **C44**(1991)2530.
- [7] J. Humblet, B.W. Fillippone, and S.E. Koonin. Phys. Rev. **C41**(1990)1736.
- [8] H. Hättig, K. Hünchen, P. Roth and H. Wäffler. Nucl. Phys. **A137**(1969)144.
- [9] H. Hättig, K. Hünchen, and H. Wäffler. Phys. Rev. Lett. **25**(1970)941.
- [10] K. Neubeck, H. Schober, and H. Wäffler; Phys. Rev. **C10**(1974)320.
- [11] F.C. Barker, *Private Communication*.
- [12] R.E. Azuma, *et al.*, Phys. Rev. **C50**(1994)1194.
- [13] Z. Zhao, R.H. France III, K.S. Lai, S.L. Rugari, M. Gai, and E.L. Wilds, Phys. Rev. Lett. **70**(1993)2066, ER **70**(1993)3524.
- [14] Z. Zhao, Ph.D. thesis, Yale University, 1993, unpublished.
- [15] Z. Zhao, L. Debrackeler, and E.G. Adelberger; 1995, *Private Communication*. These data were used by specific permission to be included in [17] and they are listed in numerical form in [17]. The data listed in Table A.2 are identical to those listed in Ref. [17] which is available on the internet.
- [16] R.H. France III, E.L. Wilds, N.B. Jevtic, J.E. McDonald, and M. Gai. Nucl. Phys. **A621**(1997)165c.
- [17] R.H. France III, Ph.D. Thesis, 1997, Yale University, unpublished, <http://bobgoyangi.gcsu.edu/France/Thesis/thesis.html>.
- [18] X.D. Tang, M. Notani, K.E. Rehm, I. Ahmad, J. Greene, A.A. Hecht, D. Henderson, R.V.F. Janssens, C.L. Jiang, E.F. Moore, R.C. Pardo, G. Savard, J.P. Schiffer, S. Sinha, M. Paul, L. Jisonna, R.E. Segel, C. Brune, A. Champagne, A. Wuosmaa; Bull. Amer. Phys. Soc. **50**,#6(2005)119.
- [19] J.F. Ziegler, *Stopping Powers and Range in all elements*, Pergamon Press, 1977.

## VI. APPENDIX

We include numerical values of other measured  $\beta$ -delayed  $\alpha$ -particle emission data sets:

Table A.1: Mainz(71) data set [8, 9, 10, 11] with  $\beta$  background subtracted.

$E_{cm}$	cts./14 keV	$E_{cm}$	cts./14 keV	$E_{cm}$	cts./14 keV	$E_{cm}$	cts./14 keV
1440	3405(450)	1793	48833(221)	2146	444856(667)	2499	682050(826)
1454	3077(433)	1807	53503(231)	2160	483692(695)	2514	620224(788)
1468	4188(346)	1821	58701(242)	2174	526321(725)	2528	563602(751)
1482	4188(346)	1835	64079(253)	2189	571892(756)	2542	510728(715)
1496	4772(303)	1849	70676(266)	2203	618339(786)	2556	459941(678)
1510	5642(256)	1863	77366(278)	2217	670463(819)	2570	413566(643)
1524	5747(266)	1878	84753(291)	2231	724409(851)	2584	371361(609)
1538	7140(213)	1892	92990(305)	2245	780412(883)	2598	333038(577)
1553	7894(207)	1906	101301(318)	2259	835509(914)	2613	299558(547)
1567	8809(187)	1920	110729(333)	2273	887989(942)	2627	268149(518)
1581	9956(177)	1934	120862(348)	2287	940716(970)	2641	240195(490)
1595	11465(166)	1948	133076(365)	2302	990074(995)	2655	214700(463)
1609	12659(163)	1962	144569(380)	2316	1035270(1017)	2669	192662(439)
1623	13843(165)	1977	157468(397)	2330	1067060(1033)	2683	173030(416)
1637	15536(164)	1991	171864(415)	2344	1093030(1045)	2697	154921(394)
1651	17367(166)	2005	188071(434)	2358	1102330(1050)	2711	137601(371)
1666	19393(167)	2019	204918(452)	2372	1103420(1050)	2726	121153(348)
1680	21678(172)	2033	223316(473)	2386	1090340(1044)	2740	106848(327)
1694	24254(177)	2047	243641(494)	2401	1065430(1032)	2754	94373(307)
1708	27143(184)	2061	264433(514)	2415	1027410(1014)	2768	83053(288)
1722	30005(185)	2075	289202(538)	2429	983372(992)	2782	73408(271)
1736	32645(195)	2090	314792(561)	2443	928649(964)	2796	65206(255)
1750	36425(191)	2104	342694(585)	2457	869743(933)	2810	57211(239)
1765	40454(201)	2118	374401(612)	2471	808732(899)		
1779	44290(210)	2132	407842(639)	2485	743730(862)		



Table A.2: Seattle(95) data set [15] as listed (by permission) in Ref. [17].

$E_{cm}$	cts./27 keV	$E_{cm}$	cts./27 keV	$E_{cm}$	cts./27 keV	$E_{cm}$	cts./27 keV
835	8(3)	1454	25(5)	2073	2141(46)	2691	1142(34)
868	13(4)	1486	28(5)	2105	2706(52)	2724	821(29)
900	16(4)	1519	55(7)	2138	3214(57)	2757	643(25)
933	10(3)	1551	68(8)	2170	3964(63)	2789	466(22)
965	12(3)	1584	64(8)	2203	4801(69)	2822	395(20)
998	11(3)	1617	111(11)	2235	5681(75)	2854	256(16)
1030	13(4)	1649	120(11)	2268	6533(81)	2887	188(14)
1063	12(3)	1682	161(13)	2301	7348(86)	2919	118(11)
1096	20(4)	1714	232(15)	2333	7870(89)	2952	111(11)
1128	10(3)	1747	236(15)	2366	8056(90)	2985	72(8)
1161	21(5)	1779	352(19)	2398	7777(88)	3017	43(7)
1193	7(3)	1812	392(20)	2431	7083(84)	3050	34(6)
1226	16(4)	1845	546(23)	2463	6000(78)	3082	17(4)
1258	13(4)	1877	675(26)	2496	4851(70)	3115	10(3)
1291	9(3)	1910	862(29)	2529	4038(64)	3147	6(2)
1323	15(4)	1942	979(31)	2561	3180(56)	3180	1(1)
1356	14(4)	1975	1241(35)	2594	2430(49)	3212	0(1)
1389	17(4)	2007	1468(38)	2627	1894(44)	3245	1(1)
1421	16(4)	2040	1753(42)	2659	1503(39)		